RESEARCH ARTICLE OPEN ACCESS

Biocompatible, Nanostructured, Chiral Polyesteramides: PNOBDME $(C_{34}H_{38}N_2O_6)_n$ and PNOBEE $(C_{26}H_{22}N_2O_6)_n$ Synthesized and Characterised as Cholesteric Liquid Crystals.

Mercedes Pérez Méndez *
** Instituto de Ciencia y Tecnología de Polímeros (CSIC), C/ Juan de la Cierva, 3. 28006 Madrid.*

ABSTRACT
Two new multifunctional polyesteramides designed as PNOBDME $(C_{34}H_{38}N_2O_6)_n$: poly[oxy(1,2-dodecane)-oxy-carbonyl-1,4-phenylene-amine-carbonyl-1,4-phenylene-carbonyl-amine-1,4-phenylene-carbonyl] and PNOBEE $(C_{26}H_{22}N_2O_6)_n$: poly [oxy(1,2-buthylene)-oxy-carbonyl-1,4-phenylene-amine-carbonyl-1,4-phenylene-carbonyl-amine-1,4-phenylene-carbonyl], are synthesized as cholesteric liquid crystal, characterized by ^{1}H and ^{13}C-NMR, COSY and HSQC and compared to precursor polyesters. Molecular models show helical polymeric chains with stereo regular head-tail, isotactic structure, explained as due to the higher reactivity of the primary hydroxyl with respect to the secondary one in the glycol through the polycondensation reaction. The two ^{1}H independent sets of signals observed for each enantiomer is attributed to two diastereomeric conformers: *gg* and *gt*, of the torsion containing the asymmetric carbon atom in the spacer. Thermal behavior of the new compounds is studied by TG and DSC analysis. Optical rotatory dispersion (ORD) is evaluated. Morphology of powdered PNOBDME exhibits homogeneous spherical clusters of about 5 μm in diameter homogeneously dispersed. When dispersed in solution, their helical molecules self-organize on metal and semiconductor surfaces. By dip coating technique both polymers self-organize in round nanoclusters about 5 nm thick, observed by AFM, after 3h and 21h grown on Si(100) substrate, deposited in conglomerates about 300 nm, 35 nm high. Both synthetic polyesteramides have proved to be biocompatible and to act as non-viral vectors in Gene Therapy, transfecting DNA to the nucleus cell. The synthetic cholesteric liquid crystal polyestereamides described here are similar to new cationic cholesteric liquid crystal polyesters also synthesized in our lab.
Keywords – Cholesteric LC; New polyesteramides; Synthetic method; NMR; Molecular Modeling.

Date Of Submission: 26-05-2019 Date Of Acceptance: 09-06-2019

I. INTRODUCTION

Liquid crystals are self-organizing systems. With increasing temperature, they do not directly go from the crystalline state into the melt but, in the middle, they undergo a mesophase state which combines the order of perfect crystals and mobility of liquids [1]. The parallel orientation of their longitudinal molecular axes is common to all mesophases (long-range orientational order). Two major classes can be distinguished: nematic (with molecular centers distributed isotropically) and smectic (molecular centers organized in layers). The special array of nematic planes stacked in a helical superstructure with a prevalent screw direction is called the cholesteric mesophase.

Cholesteric liquid crystal polyesters have received much attention in the last few years for their interesting chemical, optical, mechanical and biological properties. Due to their anisotropic formulation and amphiphilic nature, their molecules are able to self-organize and aggregate in blocks to form species with a supramolecular ordered structure which present desirable material properties.

Chiral, cholesteric liquid crystal $[C_{34}H_{36}O_8]_n$, named PTOBDME, poly[terephthaloyl-4-bis-oxybenzoate-decamethyl-ethylene], m=9 in Fig. 1, was obtained by polycondensation reaction between terephthaloyl-bis-(4-oxybenzoyl chloride) (TOBC) and DL-1,2 dodecanediol. Although only racemic materials were used in the synthesis, a cholesteric, chiral morphology, theoretically unexpected, was found. Evidence of this was obtained when a white solid, recrystallized, as the second fraction, from toluene mother liquor after the filtration of the polymer, identified as –PTOBDME, with $[\alpha]^{25}_{589}$ = -1.43 [1.538 gr/100ml, toluene] [2, 3]. The synthetic method [4, 5], based on the previously reported by Bilibin [6, 7], leads to the obtention of two or more fractions with progressively enriched diastereomeric excess, [2]. Not always the diastereomer in excess is the same

A similar result had been previously attained for liquid crystal PTOBEE $[C_{26}\ H_{20}\ O_8]_n$, m=1 in Fig. 1, also with cholesteric mesophase, obtained from the polycondensation reaction between the racemic glycol DL-1,2-butanediol and TOBC [4], with a similar mesogen as PTOBDME

but with ethyl group along the side chain. Its second fraction was isolated as –PTOBEE, with a value of $[\alpha]^{25}_{589}$ = -2.33 [0.0056 mol/l, toluene]. Its structure and diastereomeric excess had been characterized by NMR [8].

Both polymers had shown interesting technological properties. They behave both as thermotropic and lyotropic; self-assemble in nanocavities in solution, with different conformations depending on the solvent and on the concentration [3]; get adsorbed on metal surfaces with reordering of the polymer in the interface [9] and interact with biomacromolecules [10, 11, 12, 13].

Our main interest is the molecular design and chemical modifications of multifunctional cholesteric liquid crystals PTOBDME and PTOBEE, in order to obtain new chemical formulations involving new properties, holding the precursor helical macromolecular structure.

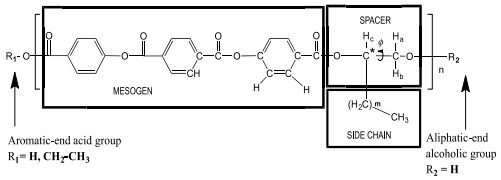

Figure 1. The monomeric unit of cholesteric liquid-crystalline PTOBEE (m=1) and PTOBDME (m=9). The three different zones of the monomer: mesogen, spacer and flexible side chain are indicated. The asterisk indicates the chiral center. Aromatic-end acid and aliphatic-end alcoholic groups are also specified.

The first feature we considered was introducing a cationic charge in the formulation of precursor PTOBDME and PTOBEE monomers, by the entrance of nitrogen atoms, giving secondary structures with long-range supramolecular order, able to interact with molecules of interest. The functional groups selected to be introduced are amide groups para-substituting the two ester groups in the central benzene ring of the terephthalate unit, along the main chain.

The final formulations of the new monomers, called PNOBDME and PNOBEE, are shown in Fig. 2(a) and 2(b) respectively. The hydrogen and carbon atoms have been numbered as precursors PTOBDME [2, 3] and PTOBEE [4, 8], respectively.

We report, the synthesis of polyesteramides PNOBDME $[C_{34}H_{38}N_2O_6]_n$ and PNOBEE $(C_{26}H_{22}N_2O_6)_n$. The structure of the polymers so obtained is confirmed by ^{1}H, ^{13}C, COSY and HSQC NMR. The spectra are quite similar to those of precursor PTOBDME and PTOBEE, as it was expected, and the shifts were assigned according to our previous notation [2] and [8]. Their thermal stability is studied by TG and DSC analysis.

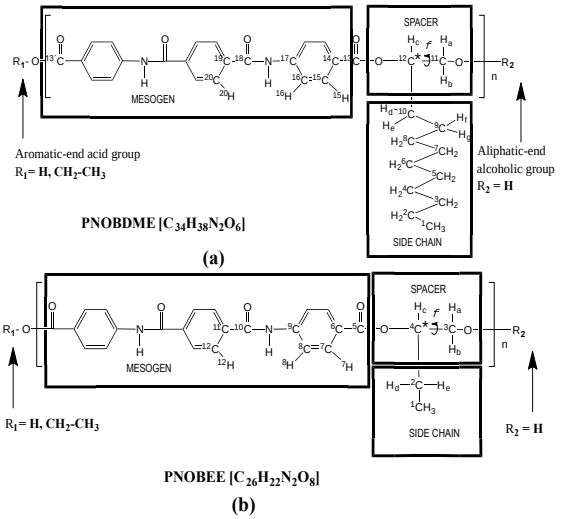

Figure 2. The monomeric unit of polyesteramides: (a) PNOBDME; (b) PNOBEE. The asterisk indicates the chiral center (^{12}C*) in PNOBDME and (^{4}C*) in PNOBEE. Torsion angle φ, along ^{11}C-^{12}C* bond and ^{3}C-^{4}C* bond, respectively, are indicated.

Their mesogens keep some similarities with Kevlar, Scheme 1, wholly aromatic polyamide, difficult to process because it's not soluble in typical solvents [14]. Instead, PNOBDME and PNOBEE contain flexible aliphatic chains that would decrease their stiffness.

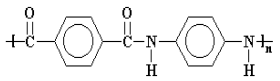

Scheme 1: Kevlar monomer

The intermediate compound of the monomeric mesogen, designed as NOBA ($C_{22}H_{16}N_2O_6$), (I in Fig. 4), was referred in the National Cancer Institute Databases with potential AIDS and cancer activity [15].

MOLECULAR MECHANICS SIMULATION OF PNOBDME.

The structural fragment including a chiral secondary alcohol and a primary alcohol group (a beta-chiral 1,2 diol) is particularly interesting since it is present in many relevant natural products, such as: sugars, nucleosides, glycerides) [16] and designed chiral nanoestructures from helical polymers and metalic salts [17].

In our case, the fragment in the spacer of PNOBDME including the secondary alcohol group, bonded to chiral ^{12}C*, and the primary alcohol, bonded to prochiral ^{11}C, is shown in Scheme 2 for the R enantiomer of ^{12}C*.

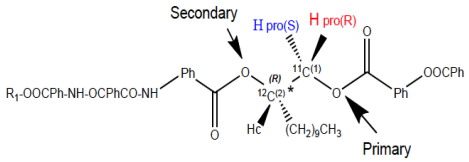

Scheme 2. Fragment in the spacer including the two alcohol groups

Molecular Mechanics, predict helical structure models for PNOBDME and PNOBEE, as formulated in Fig. 2. Instead, no helical polymer models were attained in the computational calculations when the amide group enters along the lateral side chain.

Molecular Mechanics modeling of PNOBDME monomer was developed with Materials Studio Windows v.2019 [18]. COMPASS-II Force Field was loaded, both atomic mass and charge were considered. The monomer model is shown in Fig.3(a), with its geometry optimized by minimizing the energy to 95 Kcal/mol. Monomer polymerization was simulated by considering the ^{11}C atom, in Fig. 2(a), as the head atom, and the O atom bonded to ^{13}'C, as the tail atom, being ^{12}C* the chiral center. Homopolymerization was then simulated with Head-to-Tail orientation, torsion angle between monomers fixed to 180°. Syndiotactic tacticity was finally imposed on the polymer chain. A helical polymer model along the main chain was obtained, Fig. 3(b), whose perpendicular cross section appears in Fig. 3(c).

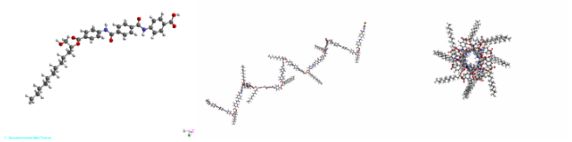

(a) (b) (c)

Figure 3. Molecular simulation of PNOBDME: (a) Minimum energy monomer; (b) Syndiotactic $[PNOBDME]_{10}$; (c) Cross-sectional view.

I. MATERIALS AND METHODS

2.1. Materials

2.1.1. Synthesis of PNOBDME [Poly[oxy(1,2-dodecane)-oxy-carbonyl-1,4-phenylene-amine-carbonyl-1,4-phenylene-carbonyl-amine-1,4-phenylene-carbonyl], $(C_{34}H_{38}N_2O_6)_n$

The new synthetic way is based on our previous experience for the obtention of cholesteric PTOBDME and a method by Sek et all [19, 20] reported for polycondensation reaction to obtain polyesteramides. In this case, we obtained an intermediate acid chloride yield lower than the obtained for the precursor polyesters.

PNOBDME, III in Fig. 4, was obtained through polycondensation reaction between 4-4´-(terephthaloyl- diaminedibenzoic chloride) NOBC, II in Fig. 4, and the racemic mixture of DL-1,2-dodecanediol. Similar notation to precursor cholesteric liquid crystal PTOBDME [2, 3] obtained by a similar method, has been used.

Starting materials: Terephthaloyl chloride from Sigma-Aldrich Chemie GmBH (Steinheim, Germany); Carbon tetrachloride from Panreac Química (Montcada i Rexach, Barcelona, Spain); NaOH from Panreac Química (Montcada i Rexach, Barcelona, Spain); 4-Aminobenzoic acid from Sigma-Aldrich Chemie GmBH (Steinheim, Germany); Hydrochloric acid from Normapur VWRInternational (Fontenay-sous-Bois, France); Thionyl chloride from Sigma-Aldrich Chemie GmBH (Steinheim, Germany); Chloroform from SDS Votre Partenaire Chimie (Peypin, France); DL-1,2-dodecanediol from Flucka Chemie GmBH (Buchs, Switzerland); Diphenyl oxide from Sigma-Aldrich Chemie GmBH (Steinheim, Germany); Nitrogen from Praxair (Madrid, Spain); Toluene from Merck KGaA (Darmstadt, Germany).

2.1.1.1 **Preparation of NOBA** (I in Fig. 4).

Solutions of 0,1 mol terephthaloyl chloride in 200 ml carbon tetrachloride and 0,2 mol NaOH in water, were added while stirring at room temperature in the course of 15 minutes, to a solution 0,22 mol of 4-Aminobenzoic acid and 0,2 mol NaOH, in 400 ml water mili-Q grade. Stirring was continued for a further 12 hr. Sediment was separated out, filtered, washed several times with 40 ml of cold water, dried, comminuted and transferred to a vessel where it was mixed for 3 hours with 300 ml of hydrochloric acid. The product was filtered, washed several times with 40 ml of cold water, dried and comminuted.
Yield 28 gr (70%).

2.1.1.2 **Preparation of NOBC** (II in Fig. 4).

In the course of 25 minutes, 15 gr NOBA was added to 350 ml thionyl chloride, while stirring rapidly at room temperature. The solution was boiled with the reflux condenser. When the liberation of HCl ended and most of the sediment had dissolved, the hot solution was filtered and cooled down to 0°C for a day. The obtained product that separated out was filtered, vacuum dried and recrystallized in chloroform.
Yield: 7,2 gr (48%).

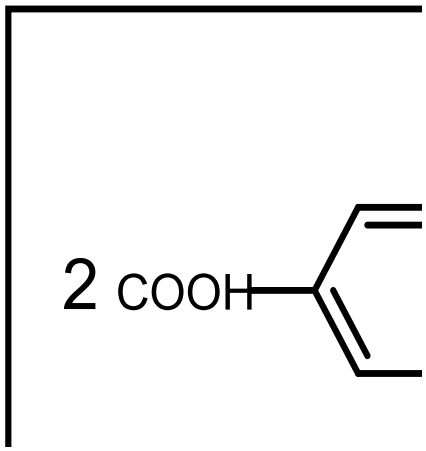

Figure 4. Scheme of polycondensation reaction of PNOBDME

2.1.1.3 **Preparation of PNOBDME**.

A mixture of 0,017 mol NOBC and 0,017 mol DL-1,2-dodecanediol, was added to 44 ml of diphenyl oxide. Purge with dry nitrogen, was used for 25 min at room temperature and then, while maintaining the gas current, the flask was transferred to a bath containing a high-temperature heat-transfer agent. The polycondensation was carried out for 3 hr. 30 min. at 200°C. The reaction finished when the liberation of HCl ended. The result of the polycondensation reaction was poured into 500 ml of toluene, decanting PNOBDME, which was filtered, washed three times with ethanol and vacuum dried. The second fraction of PNOBDME precipitated of the filtrated toluene after 22 weeks which also filtered, washed with ethanol and vacuum dried. Yield first fraction: 2,6 gr (25,5%); Yield first and second fraction: 3,1 gr (30,4%).

2.1.2. Synthesis of PNOBEE [Poly[oxy(1,2-buthylene)-oxy-carbonyl-1,4-phenylene-amine-carbonyl- 1,4-phenylene-carbonyl-amine- 1,4-phenylene-carbonyl]: ($C_{26}H_{22}N_2O_6)_n$.

PNOBEE, III in Fig. 5, was obtained through polycondensation reaction between NOBC (4-4´-terephthaloyldiaminedibenzoic chloride), II in Fig. 5, and the racemic mixture of DL-1,2-butanediol. Notation of cholesteric liquid crystal precursor PTOBEE has been used. NOBC was synthesized by the reaction between NOBA, 4-4´-(terephthaloyldiaminedibenzoic acid), I in Fig. 5, and $SOCl_2$, and recrystallized in chloroform; previously NOBA was obtained by interface condensation between terephthaloyl chloride and 4-Aminobenzoic acid.

Starting Materials: DL-1,2-butanediol from Flucka Chemie GmBH (Buchs, Switzerland); Chloronaphthalene from Sigma-Aldrich Chemie GmBH (Steinheim, Germany); Nitrogen from Praxair (Madrid, Spain); Toluene from Merck KGaA (Darmstadt, Germany).

Figure 5. Scheme of polycondensation reaction of PNOBEE.

2.1.2.1 **Preparation of PNOBEE**.

A mixture of 0,015 mol NOBC and 0,015 mol DL-1,2-butanediol, was added to 39 ml of chloronaphthalene. Purge with dry nitrogen, was used for 25 min at room temperature and then, while maintaining the gas current, the flask was transferred to a bath containing a high-temperature heat-transfer agent. The polycondensation was carried out for 180 minutes at 200°C. The reaction finished when the liberation of HCl ended. The result of the polycondensation reaction was poured into 500 ml of toluene, decanting PNOBEE, which was filtered, washed with ethanol and vacuum dried. The second fraction of PNOBEE precipitated of the filtrated toluene after 22 weeks which also filtered, washed with ethanol and vacuum dried.
Yield: 2,9 gr (46,5 %).

2.2. Characterization Techniques.

The structures of NOBA and NOBC (I and II in Fig. 4 and Fig. 5) are confirmed by conventional NMR techniques: ^{1}H-RMN, ^{13}C-NMR, COSY (Homonuclear Correlation Spectroscopy), TOCSY (Total Correlation Spectroscopy), NOESY (Nuclear Overhauser Effect Spectroscopy, through-space correlation method) and HSQC (Heteronuclear Single-Quantum Correlation spectroscopy) registered in DMSO-d_6 at 25°C in a Bruker 300MHz NMR spectrometer.

The structures of PNOBDME and PNOBEE have been confirmed by ^{1}H-RMN, ^{13}C-NMR, COSY, HSQC and HMBC (Heteronuclear Multiple Bond Correlation for correlations between carbons and protons that are separated by two, three, and, sometimes four bonds, in conjugated systems. Direct one-bond correlations being suppressed) obtained in VARIAN 400 MHz and 500 MHz spectrometers, also at room temperature. The solvent used in all cases was DMSO-d_6 from Merck KGaA (Darmstadt, Germany). ^{1}H chemical shifts were referenced to the residual solvent signal at δ = 2.50 ppm (DMSO-d_6) relative to tetramethylsilane (TMS). All the spectra were processed and analyzed with MestReNova v.11.0.3. software [21, 22].

Thermal stability measurements were studied on a Mettler TA4000-TG50 at a heating rate of 10°C/min with nitrogen purge between 30-600°C. Thermal behavior was determined by differential scanning calorimetry (DSC) in a Mettler TA4000/DSC30/TC11 calorimeter, with a series of heating/cooling cycles in a temperature range between 0- 230°C.

Microcalorimetry was evaluated in a MicroCal Inc., Model: MCS-DSC, within a range of temperature 4-120°C, at a heating rate of 10-20°C/hora, a volume of sample 1,5 ml.

The optical activity of the polymer was measured as optical rotatory dispersion (ORD) at 25°C in DMSO from Scharlau Chemie, in a Perkin Elmer 241 MC polarimeter with wavelengths: λ_{Na} = 589 nm, slit = 5 mm, integration time = 50 s; λ_{Hg} = 574 nm, slit = 14 mm, integration time = 50s; λ_{Hg} = 546 nm, slit = 30 mm, integration time = 50 s; λ_{Hg} = 435 nm, slit = 5 mm, integration time = 50s; λ_{Hg} = 365 nm, slit = 2.5 mm, integration time = 50 s.

The morphology of the samples was observed by Environmental Scanning Electron Microscope (ESEM), PHILIPS XL30.

III. RESULTS AND DISCUSSION.

3.1. Structural characterization of NOBA and NOBC by NMR.

• ^{1}H-NMR of NOBA in DMSO-d_6 at 25ºC.

Fig. 6(a) shows the ^{1}H-NMR spectrum of NOBA. The chemical shifts were assigned, according to the notation in Fig. 2(a) and Fig. 4-I, as follows.

δ (in ppm from tetramethylsilane): 12.8 (12.74) (s, 2H, C^{13}OO**H**); 10.7 (10.31) (s, 2H, ^{18}CON**H**-^{17}C); 8.11(8.18) (s, 4H, C^{20}**H**); 7.95 (8.30) (m, 4H, C^{16}**H**); 7.95 (m, 4H, C^{15}**H**). Predicted values are depicted tilted in parenthesis.

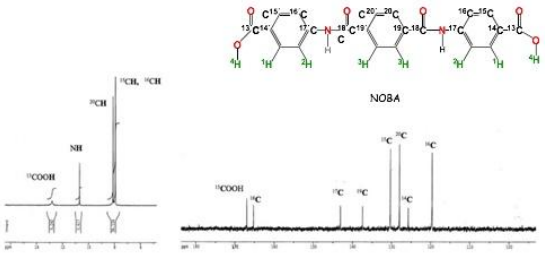

Figure 6. (a) ^{1}H- NMR Spectrum of NOBA; (b) ^{13}C-NMR Spectrum of NOBA.

Besides the protons due to ended carboxylic groups, and to amide groups, two strong signals are observed in the aromatic zone of the ^{1}H-NMR spectrum of NOBA, for to the benzene protons, ^{20}C, ^{15}C, and ^{16}C. The last two indistinguishable at 7.95 ppm.

The experimental results agree with the chemical shifts calculated by MestReNova v.11.0.3 [21, 22].

• ^{13} C-NMR of NOBA in DMSO- d_6 at 25ºC.

The ^{13}C-NMR of NOBA is given in Fig. 6(b). Their experimental chemical shifts are in complete agreement with those predicted (tilted in parenthesis).

δ (in ppm from tetramethylsilane): 167.3 (169.3) (2C ^{13}**C**OOH); 165.6 (164.7) (2C ^{18}**C**=ONH); 143.4 (143.2) (2C NH-^{17}**C**); 137.7 (134.2) (2C ^{19}**C**); 130.6 (130.5) (4C ^{15}**C**H); 128.3 (127.6) (4C ^{20}**C**H); 126.1 (125.8) (2C ^{14}**C**-COOH); 119.9 (115.8) (4C ^{16}**C**H).

• COSY OF NOBA in DMSO- d_6 at 25ºC.

The assignments of peaks in the COSY spectrum of NOBA are given in Table 1.

Table 1. COSY-NMR Assignment for NOBA

	^{1}H	^{20}H	^{15}H, ^{16}H
^{1}H		8.11	7.95
^{20}H	8.11	*	
^{15}H,^{16}H	7.95		*

• HSQC of NOBA in DMSO- d_6 at 25ºC:

The HSQC experiment (heteronuclear single quantum correlation) of NOBA appears in Fig.7, with the corresponding peaks assigned in Table 2.

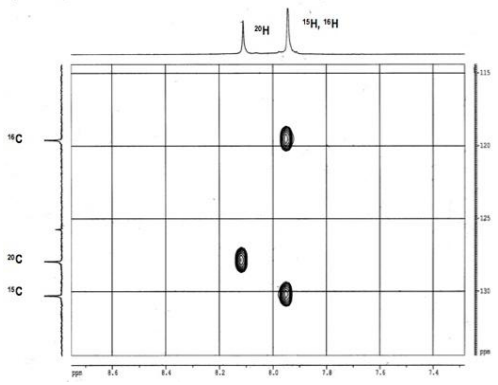

Figure 7. HSQC of NOBA

Table 2. HSQC signals of NOBA.

	^{1}H-NMR	^{20}H	^{15}H, ^{16}H
^{13}C-NMR		8.11	7.95
^{15}C	130.6		*
^{20}C	128.3	*	
^{16}C	119.9		*

Correlations between each aromatic C atom with their bonded H atoms can be confirmed. Signals due to ^{15}H and ^{16}H, overlapped in the ^{1}H spectra, can be differentiated by HSQC, and assigned to carbon atoms ^{15}C and ^{16}C respectively.

The asymmetric shape of both protons allows their differentiation. While ^{16}H slightly shifts towards lower ppm value, ^{15}H shifts to higher ppm. The integral ratio of aromatic peaks, (^{15}H+^{16}H)/^{20}H, is observed to be 2:1 in the ^{1}H spectrum, in agreement with the HSQC experiment. The structure of NOBC (Fig. 4-II), has also been confirmed by NMR experiments. Data are not given as they do not provide further information than NOBA to the present contribution.

3.2. Structuralcharacterization of polyesteramide PNOBDME by NMR.

The structure of PNOBDME, as described in Fig. 2(a), has been characterized by ^{1}H-NM, ^{13}C-NMR, COSY, TOCSY, NOESY, and HSQC, in DMSO-d_6. In Fig. 8(a) the ^{1}H- NMR spectrum is given, compared to that of PTOBDME, in Fig. 8(b). Fig. 9 exhibits the ^{13}C-NMR spectrum.

• ^{1}H-NMR: (400MHz, DMSO- d_6, 25ºC)

δ (ppm) 10,7 (s, 2H $C_{18}ON\underline{\mathbf{H}}$-C); 10,45 (m, 2H $C_{18}ON\underline{\mathbf{H}}$-C); 8,14 (s, 4H, HNCO-C-$C_{20}\underline{\mathbf{H}}$-C-CONH); 7,98 (m, 4H, COO-C-$C_{15}\underline{\mathbf{H}}$-CH-C-NHCO); 7,98 (m, 4H, COO-C-CH-$C_{16}\underline{\mathbf{H}}$-CNHCO); 5,39 (m 1H, C=OO-CH'$_a$H'$_b$-$C_{12}\underline{\mathbf{H}_c}$'-$R_1R_2$); 5,22 (m 1H, C=OO-$CH_aH_b$-$C_{12}\underline{\mathbf{H}_c}$-$R_1R_2$); 4,54 (dd 1H, J=12 Hz J=4Hz C=OO-$C_{11}\underline{\mathbf{H'}_a}H'_b$-CH'-$R_1R_2$); 4,44 (dd 1H, J=11,5 Hz J= 8Hz C=OO-C_{11}H'$_a\underline{\mathbf{H'}_b}$-CH'-$R_1R_2$); 3,91 (dd 1H, J= 12Hz J=4Hz C=OO-$C_{11}\underline{\mathbf{H}_a}H_b$-CH-$R_1R_2$); 3,83 (dd 1H, J= 12Hz J=5Hz C=OO-$C_{11}H_a\underline{\mathbf{H}_b}$-CH-$R_1R_2$); 1,85 (m 2H, CH_2-$C_{10}\underline{\mathbf{H}}_2$CH-$R_1R_2$); 1,74 (m 2H, CH_2-$C_{10}\underline{\mathbf{H}}_2$-CH'-$R_1R_2$); 1,50 (m 2H, (m 2H, $C_9\underline{\mathbf{H}}_2$-$CH_2$-CH-$R_1R_2$); 1,40 (m 2H, $C_9\underline{\mathbf{H}}_2$-$CH_2$CH'-$R_1R_2$); 1,24 (m 14H, $C_8\underline{\mathbf{H}}_2$- $C_7\underline{\mathbf{H}}_2$- $C_6\underline{\mathbf{H}}_2$- $C_5\underline{\mathbf{H}}_2$- $C_4\underline{\mathbf{H}}_2$- $C_3\underline{\mathbf{H}}_2$- $C_2\underline{\mathbf{H}}_2$-$CH_3$); 1,21 (m 14H, $C_8\underline{\mathbf{H}}_2$- $C_7\underline{\mathbf{H}}_2$- $C_6\underline{\mathbf{H}}_2$- $C_5\underline{\mathbf{H}}_2$- $C_4\underline{\mathbf{H}}_2$- $C_3\underline{\mathbf{H}}_2$- $C_2\underline{\mathbf{H}}_2$-$CH_3$); 0,86 (t 3H, CH_2-$C_1\underline{\mathbf{H}}_3$); 0,82 (t 3H, CH_2-$C_1\underline{\mathbf{H}}_3$).

• ^{13}C-NMR: (400MHz, DMSO- d_6, 25ºC)

δ (ppm) 165,2 (2C $\underline{\mathbf{C}}_{13}$=OO o 2xC $\underline{\mathbf{C}}_{18}$=ONH); 137,4 (2C HNCO-C-CH-CH-$\underline{\mathbf{C}}_{19}$-CONH); 130,3 (4C C=ONH-C-CH-$\underline{\mathbf{C}}_{15}$H-C-COO); 130,1 (4C C=ONH-C-CH-$\underline{\mathbf{C}}_{15}$H-C-COO);128,7 (4C C=ONH-C-CH-$\underline{\mathbf{C}}_{20}$H-C-C=ONH); 128,0 (4C C=ONH-C-CH-$\underline{\mathbf{C}}_{20}$H-C-C=ONH); 119,6 (4C C=ONH-C-$\underline{\mathbf{C}}_{16}$H-CH-C-COOH); 119,4 (4C C=ONH-C-$\underline{\mathbf{C}}_{16}$H-CH-C-COOH); 31,3 (1C R1R2CH-$\underline{\mathbf{C}}_{10}$H2$CH_2$); 29,0 28,8, 28,7 and 28,4 (5C C_9H_2-$\underline{\mathbf{C}}_8H_2$ $\underline{\mathbf{C}}_7H_2$-$\underline{\mathbf{C}}_6H_2$-$\underline{\mathbf{C}}_5H_2$-$\underline{\mathbf{C}}_4H_2$ -CH_2-CH_2- CH_3); 25,6 22,12 (2C $\underline{\mathbf{C}}_3H_2$-$\underline{\mathbf{C}}_2H_2$-$CH_3$); 14,0 (1C $\underline{\mathbf{C}}_1H_3$).

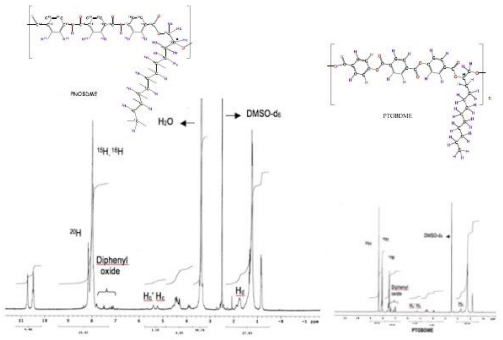

Figure 8. (a) ^{1}H- NMR Spectrum of PNOBDME. Peaks between 7- 7.8 are due to solvent impurities, diphenyl oxide, used in the synthetic process; (b) ^{1}H-NMR Spectrum of PTOBDME.

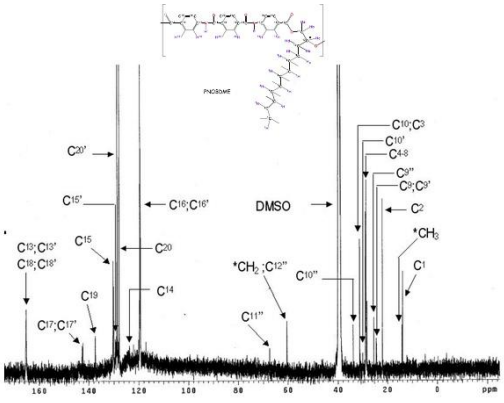

Figure 9. ^{13}C- NMR Spectrum of polyesteramide PNOBDME.

The complete assignment of the ^{1}H and ^{13}C-NMR chemical shifts for the monomeric unit and the end groups of PNOBDME are given in Table 3, together with their theoretical values calculated by

MestReNova [21, 22]. Similar notations as those assigned to precursor cholesteric liquid crystal polyesters PTOBDME [2] have been used.

The proton spectrum can be divided into three zones corresponding to the mesogen, including aromatic and amide protons between 11.0 - 7.00 ppm, the flexible side chain formed with aliphatic protons, between 2.0 - 0.5 ppm, detailed in Fig. 8(a), and the spacer with the CH_n protons directly attachment to O atoms, between 5.5 - 3.5 ppm.

The main feature of the proton spectrum is the presence of a higher number of peaks than those expected for the monomeric unit. The tetrahedral carbon atom ^{11}C, allocated in α with respect to the asymmetric carbon atom $^{12}C^*$, is referred as *prochiral* since it can be converted to a chiral center by arbitrarily changing only one attached H group to a deuterium atom (D has a higher priority than H). Depending on the configuration, R/S, of the so created chiral center, the H atom idealy deuterated, is labelled as *pro-R/S*. The two hydrogen atoms on the prochiral ^{11}C carbon atom, H_a and H_b, can be described as *prochiral hydrogens*. Prochiral hydrogens can be also designated as diastereotopic, their indistinguishable ^{1}H-NMR signals, splitting in two signals easily differentiated. The same effect is observed for H_d and H_e, bonded to prochiral ^{10}C, and for H_f and H_g, both bonded to prochiral ^9C.

The presence of two independent ^{1}H-NMR sets of signals is observed in the spectrum, one marked with one apostrophe (’) and another without it ( ). They are attributed to two conformers gg and gt of the spacer within the repeating unit respectively. The same effect has been reported for PTOBDME and PTOBEE, and accordingly similar nomenclature is used to identify the signals. The third set of signals, marked with double apostrophe (’’), is assigned to the aliphatic end group.

The main difference of the ^{1}H-NMR spectra of PNOBDME with respect to the observed for polyester PTOBDME lays in the aromatic zone due to the presence of terephthalamide in the central ring instead of terephtalate. Two peaks at 10.71 ppm and 10.48 ppm, are designated as protons N<u>H</u> and N’<u>H</u>’, theoretically expected at 10.73, splitting here either by the presence of two diastereoisomers, or by differences between the two amides environment within the monomer.

In the same mesogen zone two strong peaks, also observed in NOBA, are present in polyesteramide PNOBDME at 8.13 ppm due to benzene protons ^{20}H, and a multiplet centered at 7.95 ppm (broad and overlapped) assigned to aromatic protons (^{15}H + ^{16}H) respectively, matching respectively the calculated values (8.18 ppm for ^{20}H) and (7.98 ppm for ^{15}H and 7.95 ppm for ^{16}H). However, the proportion between integrals of both signals is 1:5, instead of 1:2. On the contrary, the three benzene protons are clearly distinguished in the case of polyester PTOBDME, see Fig. 8(b).

Detail of the zone corresponding to the spacer in the ^{1}H spectrum of PNOBDME can be seen in Fig. 10(b). Multiplets observed at 5.39 and 5.22 ppm, are interpreted as protons H_c’, H_c of the two diastereoisomers, being the diastereoisomer excess easily evaluated by their integral ratio. The peak observed at 4.35 ppm is, designated as H_c’’ in the aliphatic-OH end group. A triplet at 4.25 ppm, is assigned to the OC**H**$_2$CH$_3$ ester in the aromatic end group.

Table 3. ^{1}H and ^{13}C-NMR Chemical Shifts (ppm) observed for chiral polyesteramide PNOBDME and theoretically calculated values.

System (’)				*System ( )*				*Theoretical Shifts*			
Atom	**^{1}H**	**Atom**	**^{13}C**	**Atom**	**^{1}H**	**Atom**	**^{13}C**	**Atom**	**^{1}H**	**Atom**	**^{13}C**
^{20}H	8.03	^{20}’C	128.7	^{20}H	8.13	^{20}C	127.9	^{20}H	8.18	^{20}C	127.6
		^{19}’C	142.4			^{19}C	137.2;139			^{19}C	134.2
N’**H**’	10.48	^{18}’C	165.3	**NH**	10.71	^{18}C	165.3	**NH**	10.25	^{18}C	164.7
		^{17}’C	144.2			^{17}C	144.2			^{17}C	142.2
^{16}’H	7.975	^{16}’C	119.7	^{16}H	7.985	^{16}C	119.6	^{16}H	7.95	^{16}C	118.7
^{15}’H	7.962	^{15}’C	129.8	^{15}H	8.00	^{15}C	130.3	^{15}H	7.98	^{15}C	130.1
		^{14}’C	124.7			^{14}C	123.5			^{14}C	125.7
		^{13}’C	165.0			^{13}C	165.0			^{13}C	165.9
H_c’	5.39	^{12}’C	73.2	H_c	5.22	^{12}C	73.7	H_c	4.55	^{12}C	73.6
H_a’,H_b’	4.54;4.44	^{11}’C	65.8	H_a,H_b	3.91;3.83	^{11}C	46.7	H_a,H_b	4.80;4.55	^{11}C	64.3
H_d’,H_e’	1.79	^{10}’C	30.7	H_d,H_e	1.74	^{10}C	31.8	H_d,H_e	1.71	^{10}C	30.7
H_f’,H_g’	1.42	^{9}’C	24.6	H_f,H_g	1.34	^{9}C	24.2	H_f,H_g	1.29	^{9}C	25.3
$^{8\text{-}5}$’H	1.25	$^{8\text{-}5}$’C	28.6	$^{8\text{-}5}$H	1.25	$^{8\text{-}5}$C	28.6	$^{8\text{-}5}$H	1.29	$^{8\text{-}5}$C	29.6
^{4}’H	1.25	^{4}’C	28.4	^{4}H	1.25	^{4}C	28.4	^{4}H	1.26	^{4}C	29.3
^{3}’H	1.25	^{3}’C	31.3	^{3}H	1.25	^{3}C	31.3	^{3}H	1.26	^{3}C	31.9
^{2}’H	1.25	^{2}’C	22.1	^{2}H	1.25	^{2}C	22.1	^{2}H	1.26	^{2}C	22.7
^{1}’H	0.85	^{1}’C	13.9	^{1}H	0.86	^{1}C	13.9	^{1}H	0.88	^{1}C	14.1
Experimental signals aliphatic end group								*Theoretical Shifts End group (’’)*			
H_c’’	4.35	^{12}’’C	60.4					H_c’’	3.81	^{12}’’C	70.8
H_a’’,H_b’’	4.54;4.44	^{11}’’C	67.5					H_a’’,H_b’’	4.53;4.28	^{11}’’C	70.8
H_d’’;H_e’’	1.89;1.77	^{10}’’C	34.6					H_d’’;H_e’’	1.44	^{10}’’C	34.0
H_f’’,H_g’’	1.51;1.42	^{9}’’C	26.0					H_f’’,H_g’’	1.29	^{9}’’C	25.6
$^{8\text{-}5}$’’H	1.21	$^{8\text{-}5}$’’C	28.6					$^{8\text{-}5}$’’H	1.29	$^{7\text{-}5}$’’C	29.6
^{4}’’H	1.21	^{4}’’C	28.4					^{4}’’H	1.26	^{4}’’C	29.3
^{3}’’H	1.21	^{3}’’C	31.3					^{3}’’H	1.26	^{3}’’C	31.8
^{2}’’H	1.21	^{2}’’C	22.1					^{2}’’H	1.26	^{2}’’C	22.7
^{1}’’H	0.85	^{1}’’C	13.9					^{1}’’H	0.86	^{1}’’C	14.1

Experimental aromatic ester end group signals

CH$_2$ *	4.25	**C**H$_2$ *	60.6
CH$_3$ **	1.33	**C**H$_3$ *	14.2

In a similar way to H_c protons, three independent pairs of H_aH_b signals are also observed, due to the splitting of diastereotopic hydrogen atoms. Two for the monomer, marked with an apostrophe (’) and without it ( ), and one for the aliphatic-OH end group, marked with (’’). The double doublet at 4.54 ppm and the very complex signal at 4.44 ppm are attributed to H_a’ and H_b’ respectively, and the pair of double doublets at 3.91, 3.83 ppm are interpreted as H_a and H_b. The signal at 4,44 would be formed by one double doublet overlapped with a pair of double doublets.

The integral ratio between peaks H_c’ (5.39 ppm) and H_a’ (4.54 ppm) gives a ratio 1:1. Peaks H_c (5.22 ppm), H_a (3.91 ppm) and H_b (3.83 ppm) present a ratio 1:1:1. The TOCSY experiment will confirm these assignations and will resolve the overlapped signal at 4.44 ppm. The aliphatic zone, in

Fig. 8(a), exhibits multiplets centered at 1.89, 1.77, 1.51, 1.42, 1.25 and 0.86. The last two are directly assigned to (CH_2) and CH_3, among the first four, only two were predicted. They are resolved also by TOCSY. All these signals were also observed for PTOBDME.

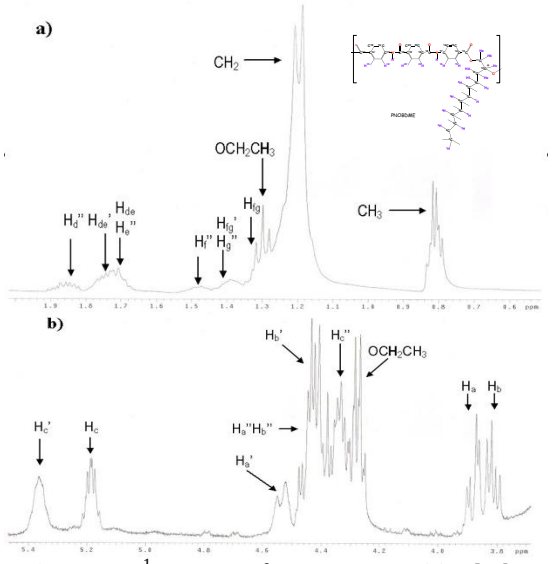

Figure 10. ^{1}H-NMR of PNOBDME: (a) Aliphatic chain zone; (b) Spacer zone.

The ^{1}H-^{1}H- TOCSY 2D experiment, in Fig. 11, shows the correlations between the proton signals H_c', H_c and H_c" with their respective coupling networks, hence confirming the presence of three independent sets of signals.

Besides, the multiplets overlappings due to spin-spin coupling can be resolved: at 4.44 ppm in signals H_a'', H_b'' and H_b'; at 1.77 ppm distinguishing signals H_dH_e, H_d'H_e' and H_e''; at 1.44 ppm as due to signals H_f'H_g' and H_g''. Even a new signal at 1.34 corresponding to H_f H_g could be observed.

The experiment COSY confirmed the assignment with the correlation of double doublets at 4.54 ppm (H_a') and 4.44 ppm (H_b') with multiplet H_c' at 5.39 ppm, and this with 1.79 ppm (H_d'H_e'), and this with 1.42 ppm (H_f' H_g'). The same correlation is found with double doublet at 3.91 ppm (H_a) and 3.83 ppm (H_b) with 5.22 ppm (H_c), and this with 1.74 ppm (H_dH_e), and finally with 1.34 ppm (H_fH_g). COSY did not let identify the end group overlapping signals.

Correlation between aromatic and amide protons of PNOBDME can be elucidated by ^{1}D-NOESY experiment, in Fig. 12.

When irradiated at 10.71 ppm, the peak N**H** shows positive NOE with ^{20}H (8.13 ppm) and with ^{16}H (7.985 ppm). Irradiated at 10.48 ppm, N'H' shows positive NOE with ^{20}'H (8.03 ppm) and with ^{16}'H (7.975 ppm). The ^{1}D-NOESY irradiated at 1.74, H_dH_e showed a broad positive NOE with ^{15}H (8.00 ppm).

These correlations of the aromatic protons with the amide protons and aliphatic would explain the (1:5) proportion observed between the signal at 8.13 and overlapped signal centered at 7.97, previously mentioned. More precise differentiation and assignation between of ^{16}H and ^{16}'H and also ^{15}H and ^{15}'H is hard to be performed with this technique, due to overlapping.

Similarly to the changes between the integral proportion of signals H_c: H_c' in the first and second fraction of PNOBDME, different amide protons ratio N**H**: N'**H**' can be distinguished in different polymer fractions.

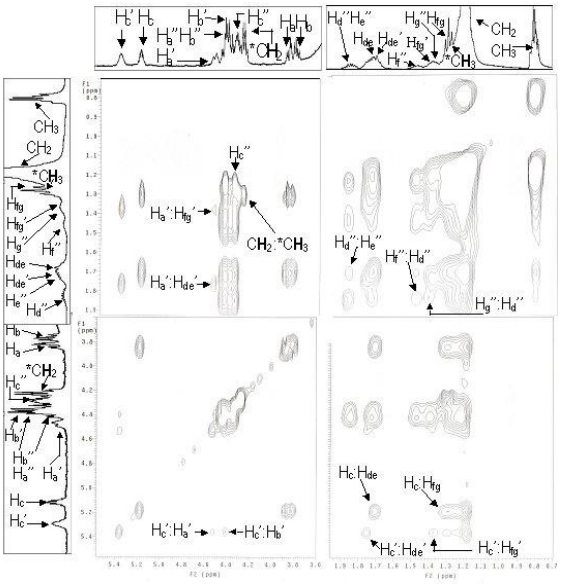

Figure 11. ^{1}H-^{1}H -TOCSY 2D experiment of PNOBDME.

The assignment of carbons directly bonded to protons is carried out by the HSQC experiment, in Fig. 13. Correlation between protons H_a'(4.54 ppm) and H_b'(4.44 ppm) with the same carbon atom ^{11}'C (65.8 ppm) is confirmed. Within proton multiplet around 4.44 ppm, carbon atom ^{11}''C (67.5 ppm) is connected with signals H_a'' and H_b'' (4.44 ppm), indiscernible in the proton experiments. The correlation between H_a (3.91 ppm) and H_b (3.83 ppm) with carbon atom ^{11}C at (46.7 ppm) is also observed.

The complex signal of proton centered at 1.77, solved in the TOCSY experiment, is also resolved in HSQC, by three correlation signals between H_d'H_e' (1.79 ppm) with carbon ^{10}'C at (30.7 ppm) and H_d H_e (1.74 ppm) with carbon ^{10}C (at 31.8 ppm); and H_e'' (1.77 ppm) with carbon ^{10}''C (34.6 ppm) which is also correlated with H_d''(1.89 ppm).

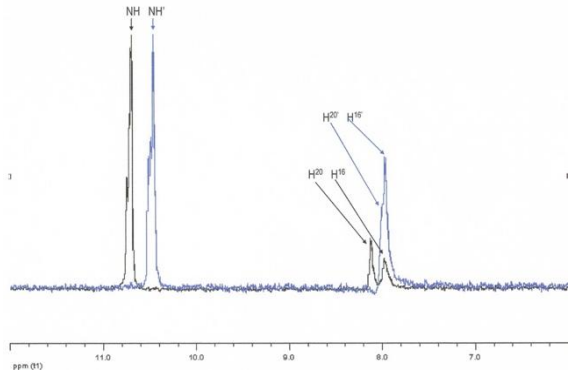

Figure 12. ^{1}D-NOESY of PNOBDME, blue irradiated at 10.48 and black irradiated at 10.71.

Multiplet around 1.44 can be solved by distinguishing correlation between protons H_f'H_g'(1.42 ppm) with carbon ^{9}'C (24.6 ppm) and H_f H_g (1.34 ppm) with ^{9}C (24.2 ppm). Additionally, carbon ^{9}''C (26.0 ppm) also correlates with H_f''(1.51 ppm) and H_g''(1.42 ppm), in agreement with the TOCSY results. In the aromatic zone, the assignation of ^{20}'H (8.03 ppm) and ^{20}H (8.13 ppm) is confirmed and these signals presented correlation with ^{20}'C (128.7 ppm) and ^{20}C (127.9 ppm) respectively. Two broaden correlations are observed between ^{15}'H (8.0 ppm) and ^{15}'C (130.3 ppm) and between ^{16}H (7.980 ppm) and ^{16}C (119.6 ppm).

In HMBC experiment, Fig. 14, with correlations carbon-proton separated by two, three, and, even four bonds apart, the HSQC broaden correlations between aromatic ^{15}H and ^{15}C, and ^{16}H and ^{16}C can be resolved and related to the sets of signals with apostrophe (') and without it ( ). Additionally, carbonyl and quaternary carbons atoms are also confirmed by HMBC.

In HMBC, the following cross signals are observed: ^{16}C (119.7 ppm) correlates with N**H** (10.71 ppm) and also with ^{15}H (8.00 ppm); Signal ^{16}'C (119.6 ppm) causes correlation with N'**H**' (10.48 ppm) and also with ^{15}'H (7.962 ppm); Signal ^{15}H (8.00 ppm) correlates with ^{14}C (123.5 ppm) and with ^{17}C (144.2 ppm); Signal ^{16}H (7.985 ppm) correlates with ^{14}C (123.5 ppm) and ^{17}C (144.2 ppm) and ^{15}C (130.3 ppm); Signal ^{15}'H (7.962 ppm) also presented another correlation with ^{14}'C (124.7 ppm).

Correlation between ^{16}'H signals (7.975 ppm) and ^{15}'C (129.6 ppm) was confirmed and another cross signals of ^{16}'H with ^{14}'C (124.7 ppm); ^{16}'H also showed correlation with ^{17}C (144.2 ppm) as ^{16}H; ^{20}H (8.13 ppm) correlates with ^{20}C (127.9 ppm) and with two carbon atoms at ^{19}C (137.2 ppm) and (139.1 ppm). It also correlates with ^{18}C (165.3 ppm); ^{20}'H at 8.03 exhibits correlation with ^{20}'C (128.7 ppm), with ^{19}'C (142.35 ppm) and ^{18}C (165.3 ppm), the last carbon atom not resolved; The signal at 165.3 ppm, also showed two more cross signal with NH at 10.71 ppm and NH' at 10.48 ppm; ^{13}C carbonyl carbon was observed at 165.0 with broadening and not resolved cross signal with H^{16}, $H^{16'}$, H^{15}, $H^{15'}$. Carbonyl carbon of ester aromatic end group was observed at 167.0.

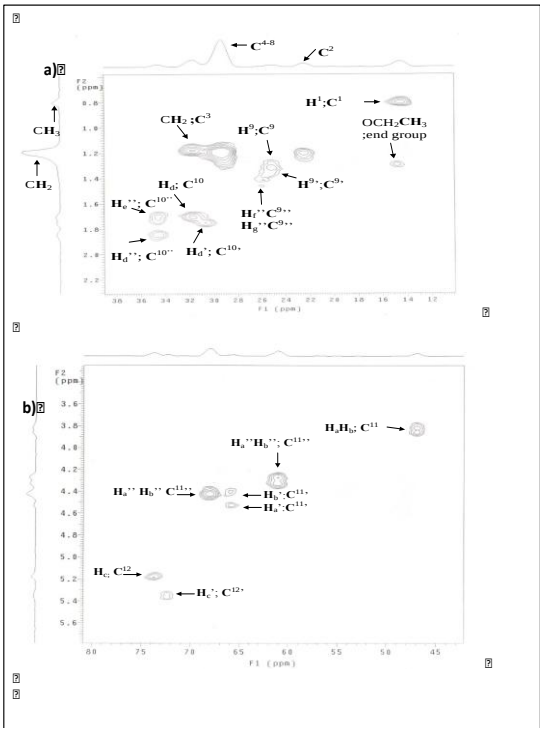

Figure 13. HSQC-NMR experiment of PNOBDME: (a) Detail of aliphatic flexible side chain; (b) A detail of the spacer zone.

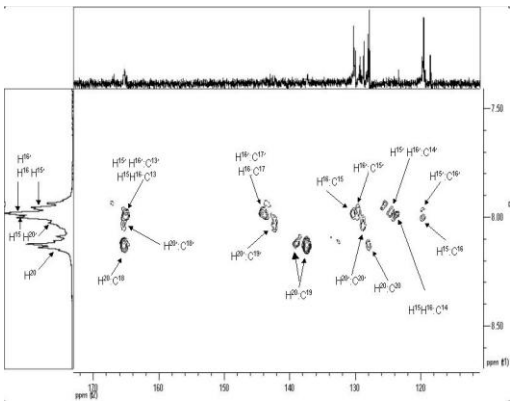

Figure 14. HMBC experiment of PNOBDME.

3.3. Structuralcharacterization of polyesteramide PNOBEE by NMR.

The structure of PNOBEE, as designed in Fig. 2(b), has been characterized by ^{1}H-NMR, ^{13}C-NMR, COSY, TOCSY, NOESY and HSQC, in DMSO-d_6.

The complete assignment of the ^{1}H and ^{13}C-NMR chemical shifts for the monomeric unit and the end groups of PNOBEE, resolved in a similar way to

that of PNOBDME, is summarized in Table 4, together with their theoretical values calculated by MestReNova [19, 20]. Similar notations to those assigned to precursor cholesteric liquid crystal polyesters PTOBEE have been used [4, 8].

In the ^{1}H-NMR spectrum of PNOBEE, the two amidic protons NH and N'H'are observed as singlets at 10.48 ppm and 10.72 ppm, respectively. At 8.14 ppm and 8.03 ppm, aromatic protons ^{12}H and ^{12}'H are identified, while ^{7}H and ^{8}H signal are broadly overlapped at 7.98 ppm, similarly to PNOBDME. The integral relation between signals at 8.14 ppm and 7.98 ppm is 1:3 instead of 1:2, since the signal at 8.03 ppm is partially overlapped with the signal at 7.98. The complete assignment of these signals was realized with other NMR experiments.

In the proton spacer zone, two multiplets observed at 5.32 ppm and 5.15 ppm, are assigned to protons H_c' and H_c, respectively, within the monomeric unit, according to the terminology previously used for PNOBDME. A double doublet at 4.55 ppm is assigned to H_a'. A broad and overlapped signal centered at 4.50 ppm should correspond with overlapping of double doublet H_b' and the double doublets H_a''H_b'' in the aliphatic end-group. A multiplet observed at 4.32 ppm is assigned to H_c" of the aliphatic end group and quadruplet at 4.28 ppm to **C**H_2 of ethyl ester end group. Finally, double doublet at 3.93 ppm and 3.87 ppm are assigned to H_a and H_b.

The observed aliphatic signals corresponding with the lateral side chain are a multiplet at 1.89 ppm and a broaden overlapped signal at 1.78 ppm interpreted as H_d, totally assigned with the help of COSY and TOCSY experiments. Triplet at 1.33 ppm is assigned to methyl or ethyl ester end group. While triplets at 1,03, 1,01 and 0,92 corresponding to H_d were also assigned with COSY and TOCSY experiments to H_e'', H_e' and H_e, respectively.

In the COSY experiment, the expected correlation between ^{12}H (8.14 ppm) and ^{8}H (7.99 ppm) is overlapped and it is indistinguishable. Signal H_c' (5.32 ppm) shows correlation with H_a' (4.55 ppm), with signal H_b' (4.47 ppm) and with signal H_d'(1.80 ppm). Signal H_c (5.15 ppm) correlates with H_a (3.93 ppm), H_b (3.87 ppm) and with H_d (1.78 ppm). The signal corresponding to H_c''(4.35 ppm) correlates with H_d'' (1.95 ppm), with H_e'' (1.76 ppm) and with H_a''H_b'' overlapped at (4.47 ppm). The signal at 4.28 ppm due to CH_2 ethyl in ester end group shows correlation with triplet at 1.33 ppm due to CH_3 in the same end group. Signal H_d'' (1.95 ppm) and H_e'' (1.76 ppm) show correlation with Hf'' (1.03 ppm). In the TOCSY spectrum, of the aromatic zone correlation of amidic proton N**H** (10.72 ppm) with ^{12}H (8.14 ppm) and ^{8}H (7.99 ppm) is observed. Also between amidic proton N'**H**' (10.48 ppm) and the overlapped signal of ^{12}'H (8.03 ppm) and ^{8}'H (7.99 ppm).

Table 4. ^{1}H and ^{13}C-NMR Chemical Shifts (ppm) observed and calculated for the repeating unit and aliphatic end group of chiral polyesteramide PNOBEE.

Set of signal of systems (') and ('')				Set of signals system without apostrophe ( )				Calculated chemical shifts	
Atom	*^{1}H(ppm) DMSO*	*Atom*	*^{13}C(ppm DMSO*	*Atom*	*^{1}H(ppm) DMSO*	*Atom*	*^{13}C(ppm) DMSO*	*Atom ^{1}H*	*Atom ^{13}C*
^{12}'H	8.03	^{12}'C	129.2	^{12}H	8.14	^{12}C	128.4	8.18	127.6
		^{11}'C	129.4			^{11}C	131.6		137.6
N'H'	10.48	^{10}'C	163.3	NH	10.72	^{10}C	163.3	10.25	164.7
		^{9}'C	143.2			^{9}C	142.8		140.1
^{8}'H	7.99	^{8}'C	119.9	^{8}H	7.99	^{8}C	120.1	7.95	121.5
^{7}'H	7.98	^{7}'C	130.8	^{7}H	7.98	^{7}C	130.8	7.88	130.1
		^{6}'C	128.7			^{6}C	125.8		125.7
		^{5}'C				^{5}C			165.9
H_c'	5.32	^{4}'C	73.0	H_c	5.15	^{4}C	74.2	4.55	72.5
H_a',H_b'	4.55,	^{3}'C		H_a, H_b	3.93, 3.87	^{3}C	46.5	4.80, 4.55	67.2
H_d'	1.80	^{2}'C	24.0	H_d	1.78	^{2}C	24.9	1.75	23.5
H_e'	1.01	^{1}'C	10.0	H_e	0.92	^{1}C	9.9	0.96	7.8
Experimental signals aliphatic end group								*Theoretical Shifts End group ('')*	
H_c''	4.32	^{4}''C	62.5					3.81	73.0
H_a'',	4.47 *	^{3}''C	67.7					4.53, 4.28	70.5
H_d'',	1.95,	^{2}''C	27.9					1.48	26.8
H_e''	1.03*	^{1}''C	11.1					0.96	7.6

Overlapped signal

End group O-**C**H_2-CH_3: 4.28 ppm (^{1}H-NMR) and 60.2 ppm (^{13}C-NMR); **C**H_3: 1.33 ppm (^{1}H-NMR) and 14.4 ppm (^{13}C-NMR)

The signal H_c'(5.32 ppm) correlates with H_d' (1.80 ppm) and H_e' (1.01 ppm). The set of signals of aliphatic-OH end group was also resolved by the correlation of H_c'' (4.35 ppm) with H_a'' H_b'' (4.47 ppm), with H_d'' (1.95 ppm), with He'' (1.76 ppm) and with Hf '' (1.03 ppm).

In the NOESY-2D experiment, the same correlations as in TOCSY-2D were observed, only correlation between H_c' (5.35 ppm) with ^{7}'H (7.98 ppm) and H_b' (4.47 ppm) with ^{8}'H (7.99 ppm). The correlations between H_c (5.15 ppm) and ^{8}H and H_a and H_b with ^{7}H were not observed. This could be indicative of a closed structure for the system ('') than for ( ) system.

After proton assignment, carbon atoms bonded directly to hydrogens were identified by the HSQC experiment. ^{12}'C (129.2 ppm) was related with ^{12}'H (8.03 ppm), and ^{12}C (128.4 ppm) with ^{12}H (8.14 ppm); ^{8}'C (119.9 ppm) and ^{8} C (120.1 ppm) with ^{8}'H and ^{8}H (7.98 ppm); ^{7}C (130.8 ppm) is related with ^{7}H (7.98 ppm); H_c' (5.32 ppm) shows correlation with ^{4}'C (73.0 ppm), while H_c (5.15 ppm) with ^{4}C (74.2 ppm); H_a (3.93 ppm) and H_b (3.87 ppm) correlates with carbon ^{3}C (46.5 ppm). ^{2}C (24.9 ppm) is related with H_d (1.78 ppm) and ^{1}C (9.9 ppm) with H_e (0.92 ppm); ^{1}'C (10.0 ppm) with H_e' (1.01 ppm). Signals due to OH-aliphatic end group: H_c'' (4.32 ppm) is related with ^{4}''C (62.5 ppm); H_a''H_b'' (4.47 ppm) with ^{3}''C (67.7 ppm); H_d'' (1.95 ppm) and H_e'' (1.76 ppm) with ^{2}''C (27.9 ppm) and H_f '' (1.03 ppm) with ^{1}''C (11.1 ppm); signal due to ester ethyl group **C**$\mathbf{H_2}$ (4.28 ppm) with ^{13}C (60.2 ppm) and **C**$\mathbf{H_3}$: ^{1}H (1.33 ppm) with ^{1}C (14.4 ppm).

3.4. Conformational analysis of PNOBDME and PNOBE

By using a Karplus type equation [23], the vicinal coupling constants $^3J_{Ha\text{-}Hc}$ and $^3J_{Hb\text{-}Hc}$ can be related with the two possible staggered conformers, *gg* and *gt* of torsion φ along $^{11}C\text{-}^{12}C^*$ bond in PNOBDME, and $^3C\text{-}^4C^*$ in PNOBEE, along the polymer backbone, Fig. 15, being m=9 for PNOBDME and m=1 for PNOBEE. In the system designed without an apostrophe ( ), the coupling constants $^3J_{Ha\text{-}Hc}$ (3.7 Hz) and $^3J_{Hb\text{-}Hc}$ (6.0 Hz) indicate the preference for *gt* conformer.

In the system with an apostrophe (’), $^3J_{Ha'\text{-}Hc'}$ cannot be measured accurately because the peak is not resolved but it is low enough to let us assure the preference of the *gg* conformer; $^3J_{Hb'\text{-}Hc'}$ cannot be measured due to the overlapping of H_b’ signal with those of H_a’’ and H_b’’. The existence of these two independent conformers had also been observed for PTOBDME and PTOBEE and it was also related with the presence of helical structures, the Cotton effect and the sign of the helicity in 1-2 di-O-benzoylated sn-glycerols [24-27]. The combination of a helix with two screw senses and the two absolute configurations by the presence of the asymmetric carbon atom, provide four diastereomeric structures, two pairs of enantiomers which would present two independent set of signals by NMR [28-32].

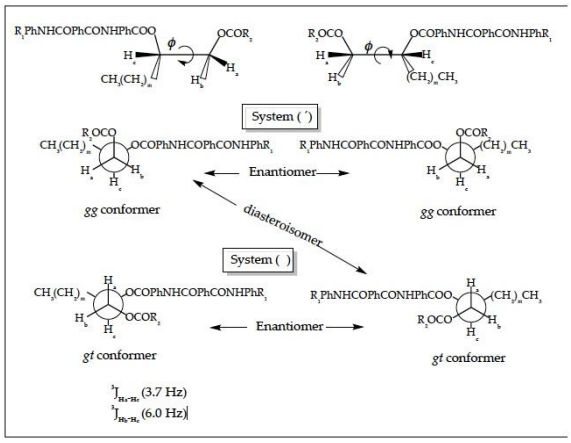

Figure 15. The relationship between the four helical conformations *gg* and *gt* of PNOBDME, and PNOBEE through the $^{11}C\text{-}^{12}C^*$ bond, and $^3C\text{-}^4C^*$ (torsion φ), respectively. The calculated vicinal coupling constant $^3J_{Ha\text{-}Hc}$ and $^3J_{Hb\text{-}Hc}$.

Details of molecular models for *gg* and *gt* conformers of a dimer of PNOBDME are shown (Fig. 16), projected along the $^{11}C\text{-}^{12}C^*$ bond, torsion φ, (perpendicular to the paper) with $^{12}C^*$ (bonded to H_c) having R and S absolute configuration, in yellow, behind ^{11}C (bonded to H_a and H_b).

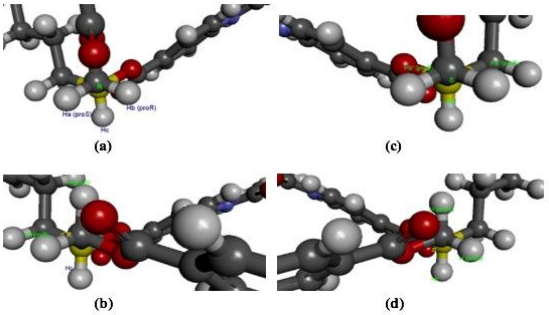

Figure 16. Molecular model details of a PNOBDME dimer. View along $^{11}C\text{-}^{12}C^*$ bond (perpendicular to the paper), with (R) and (S) absolute configuration $^{12}C^*$, in yellow behind ^{11}C, for:
(a) R*gg*-diasteroisomer; (b) R*gt*- diasteroisomer; (c) S*gg*- diasteroisomer; (d) S*gt* diasteroisomer.

Thermal Behavior

3.5.1. Thermal Stability and Differential Scanning Calorimetry of PNOBDME.

The presence of amide groups within the mesogen of PNOBDME causes a 10% weight loss at 310°C in the thermal gravimetric curve (Fig 17a) increasing of thermal stability range of precursor polyester PTOBDME, with the same weight loss percentage at 280°C [3].

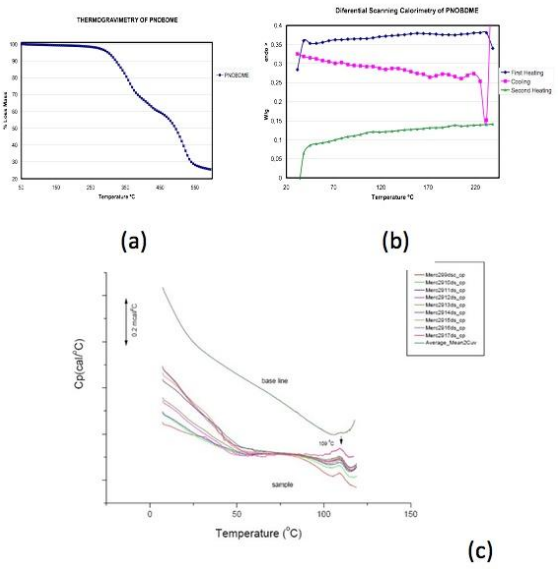

Figure 17. (a) The thermogravimetric curve of PNOBDME, first fraction; (b) DSC analysis of PNOBDME first fraction; (c) Microcalorimetry of PNOBDME.

The DSC experiment of PNOBDME, performed at 10°C/min rate (Fig. 17b) shows in the first heating run a glass transition at 62.5°C together

with a small broad endothermic peak centered at 155.7°C. During the cooling, an exothermic peak at 183°C is indicative of crystallization from the mesophase state, higher value than that of PTOBDME (149°C). In the second heating, glass transition is observed at 71.6°C, and two broad and small endothermic peaks at 108.7 and 188.3°C.

In a subsequent experiment PNOBDME was heated of up to 230°C at 10°C/min, cooled to 190°C and isothermally heated for 2 hours at this temperature, cooled to 30°C at 10°C/min, and finally heated again to 230°C, at 10°C/min. The isothermal treatment at 190°C after cooling from 230°C, should have produced an induced crystallization process, and an endothermic peak due to the polymer transition to mesophase should have been observed, however only a small endothermic peak at 109°C is observed not caused by the isothermal cooling. This endothermic transition at 109°C was also confirmed by Microcalorimetry (Fig.17c).

3.5.2. Thermal Stability and Differential Scanning Calorimetry of PNOBEE.

PNOBEE thermal stability is given in Fig.18a. A 10% weight loss due to thermal decomposition is observed at 330°C, a higher temperature than that observed for PTOBEE at 280°C [4] and PNOBDME at 310°C. The substitution of the ester group in the mesogen by amide caused the increase of thermal stability with respect to PTOBEE.

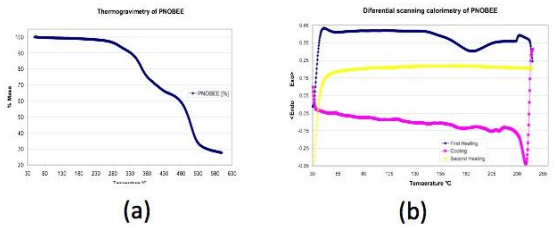

Figure 18. (a) The thermogravimetric curve of PNOBEE first fraction; (b) DSC analysis of PNOBEE first fraction.

In the DSC experiment performed at 10°C/min rate (Fig. 18b) a glass transition is observed during the first run, around 55°C, and very broad endothermic peak centered at 185,3°C interpreted as the fusion due to transition from crystal to liquid-crystal, another endothermic peak at 233,7°C is observed near the beginning of thermal decomposition; in the cooling run two small exothermic peaks appear at 205,6°C and 183,0°C due to crystallization processes from the mesophase state. In the second heating, no transition is observed.

Compared with PTOBEE, with the transition to mesophase at 149°C and with exothermic crystal formation at 110°C during isothermal heating, a remarkable difference is observed due to the substitution of ester by amide groups in the mesogen.

3.6. Optical characterization.

Although synthesized from starting racemic materials PNOBDME showed unexpected chirality. The first fraction of the polymer did not show a net optical activity but values changing from positive to negative, but the second fraction presented a low but constant value +1.02°, at 598 nm; +1.65°, at 579 nm; and +2.9°, at 435 nm, and very high optical activity between +600° or +950°, at 365 nm, depending on the temperature. This behavior was also observed in PTOBDME and PTOBEE.

Optical Rotatory Dispersion (ORD) values (α) of second fraction of PNOBDME are expressed (Fig. 19) as Molar Optical Rotation [Φ] = [α] M/100, being M the molecular weight of the polymer repeating unit, a function of time, at 365 nm, at two different temperatures: 35°C and 25°C.

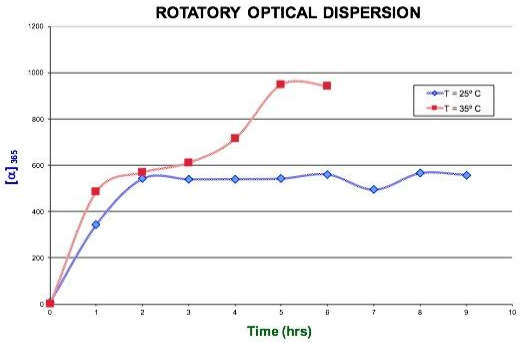

Figure 19. Optical Rotatory Dispersion (ORD) of PNOBDME second fraction at 25°C and at 35°C.

At 35°C the ORD of PNOBDME increases with time to a approximate value of 600°, which remains between 90 to 180 minutes. After that it increasses again to reach a value of 950°, after 360 minutes getting stabilized. At 25°C, after 120 minutes the ORD reaches a value of 600° that was maintained up to 9 hours.

In both cases, once the ORD value was stabilized to 600° and 950° respectively, if the lamp wavelength was changed to 435 nm and quickly returned to 365 nm, the ORD value initially decreased to +8.6 and recovered its value. This phenomenon could be totally reversible. The variation of ORD with time has been described in helical polyguanidines synthesized starting from chiral monomers or starting achiral monomers with chiral catalysts [27, 28, 29 -31].

Optical characterization of PNOBEE. At the end of this article, the optical activity of PNOBEE has not been studied.

3. 7. Morphology.

The morphology of powdered PNOBDME without any previous treatment has been studied by SEM. Four details are shown (Fig.20) of the homogeneous spherical clusters of about 5 μm in diameter homogeneously dispersed.

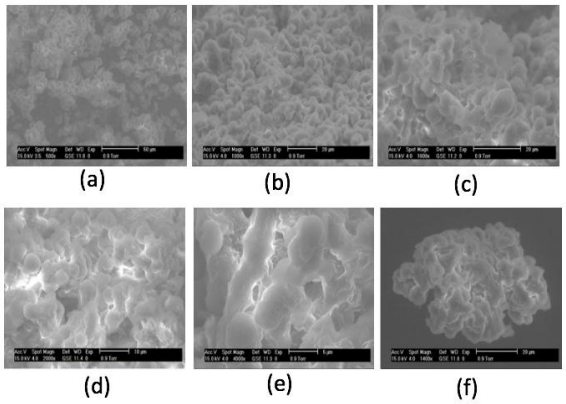

Figure 20. SEM images of powdered PNOBDME.

When dispersed in aqueous solution, their helical molecules self-organize on metal and semiconductor surfaces, such as: Si (111), Pt / TiO2 / SiO2 /Si (001), Ag, Au [9].

By dip coating technique, both polymers assemble on Si(100) substrates, previously washed with (Cl_3Et + acetone + methanol + deionized H_2O) and with (NH_4F/FH) to eliminate oxide. After 3h, and 21h, AFM (Fig. 21) shows round clusters about 5 nm thick, deposited in conglomerates about 300 nm, 35 nm high.

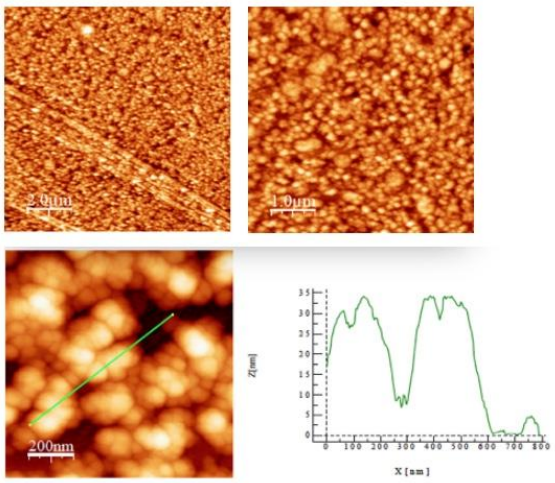

Figure 21. AFM pictures of PNOBDME deposited on Si(100) substrate by dip coating.

IV. CONCLUSIONS

The synthetic methods of two new multifunctional cholesteric liquid crystal polyesteramides designed as PNOBDME: $(C_{34}H_{38}N_2O_6)_n$ and PNOBEE $(C_{26}H_{22}N_2O_6)_n$ are reported and their characterization by ^{1}H and ^{13}C-NMR, COSY and HSQC, is stated and compared to their precursor polyesters PTOBDME and PTOBEE. Molecular models of the new polymers show helical polymeric chains.

The NMR analysis, in agreement with the Molecular Mechanics models, let us conclude that the enantiomeric polymer chains present stereo regular head-tail, isotactic structure, explained in terms of the higher reactivity of the primary hydroxyl with respect to the secondary one in the glycol through the polycondensation reaction.

In agreement with our previous experience, each enantiomer, with two independent sets of signals observed by ^{1}H and ^{13}C-NMR, differentiated with an apostrophe (’) and without it ( ), could be attributed to two diastereomeric conformers: gg and gt, related with two possible staggered conformations of the torsion angle φ, along ^{11}C-^{12}C* bond in PNOBDME and ^{3}C-^{4}C* bond in PNOBEE, respectively, with asymmetric carbon atoms (^{12}C*) and (^{4}C*) in the secondary alcohol group, along the copolymer backbone, with two possible helical screw sense of the polymer chain, for all the studied polymers. Chirality in racemic precursor PTOBDME was proposed to be due to the kinetic resolution of a preferable helical diastereomer, such as Sgt, with respect to the possible four forms, while the R/S ratio of asymmetric carbon atoms remained 50:50.

The thermal behavior of the synthesized liquid crystal polyesteramides, studied by TG and DSC analysis, show an endothermic peak assigned to the first order transition from the crystalline phase to liquid crystal mesophase.

Optical ORD values are provided for polyestereamide PNOBDME. The unexpected chirality is evaluated. The first fraction of the polymer did not show a net optical activity but values changing from positive to negative, but the second fraction presented a low but constant value +1.02°, at 598 nm; +1.65°, at 579 nm; and +2.9°, at 435 nm, and very high optical activity +600° to +950°, at 579 nm, when increasing temperature from 25C to 35C.

Morphology of powder PNOBDME is reported by ESEM, showing the homogeneous spherical clusters of about 5 μm in diameter homogeneously dispersed.

By dip coating, PNOBDME self-organize in round nanoclusters about 5 nm thick, observed by AFM, after 3h and 21h grown on Si(100) substrate, deposited in conglomerates about 300 nm, and 35 nm high.

The synthetic cholesteric liquid crystal polyestereamides described here are similar to new

cationic cholesteric liquid crystal polymers also synthesized in our lab [33].

ACKNOWLEDGEMENTS

The author thanks CSIC by the financial support to the Project "Nuevos vectores no virales basados en polímero cristal-líquido colestérico (PCLC) y su uso para transfección génica", PTR1995-0760-OP de Estímulo a la Transferencia de Resultados de Investigación PETRI. The author thanks Dr Javier Sanguino for his valuable help.

REFERENCES:

[1]. H. Ringsdorf; B. Schlarb; J. Venzmer, Molecular architecture and function of polymeric oriented systems: models for the study of organization, surface recognition, and dynamics of biomembranes. Ang. Chem. Int. Ed. Engl. 1988, 27, 113.

[2]. M. Pérez Méndez; J. Sanguino Otero, Cholesteric Liquid-Crystal Copolyester, Poly[oxycarbonyl-1,4-phenylene- oxy - 1,4 terephthaloyl- oxy- 1,4-phenylene- carbonyloxy (1,2-dodecane)] [C34H36O8]n, Synthesized from Racemic Materials: Kinetics, Structure and Optical Characterization, International Journal of Engineering Research and Applications (IJERA) July 2015, Vol. 5, Issue 7, (Part -2), pp. 48-62, ISSN: 2248-9622, http://www.ijera.com/papers/Vol5_issue7/Part%20-%202/H57024862.pdf

[3]. J. Fayos; S. Sanchez-Cortes; C. Marco; M. Pérez-Méndez, Conformational analysis and molecular modelling of cholesteric liquid crystal polyesters based on XRD, Raman, and Transition thermal analysis. J. Macromol. Sci. B: Phys. 2001, 40, 553-576.

[4]. M. Pérez-Méndez; C. Marco, New synthesis, thermal properties and textures of cholesteric: Poly[oxy (1,2-butene)oxycarbonyl-1,4-phenylene oxycarbonyl-1,4-phenylenecarbonyloxy- 1,4-phenylenecarbonyl], PTOBEE, Acta Polym. 1997, 48, 502-506.

[5]. M. Pérez-Méndez; C. Marco Rocha, Process for obtaining cholesteric liquid crystals by stereoselective recrystallization. Patents: EP1004650-A, WO9831771-A, WO9831771-A1, AU9854863-A, ES2125818-A1, US6165382-A, MX9906732-A1, JP2001513827-W, AU739076-B, DE69824182-E.

[6]. A.Y. Bilibin,; A.V. Ten´kovtsev,; O.N. Piraner,; S.S. Skorokhodov, Synthesis of high molecular weight liquid crystal polyesters based on a polycondensation mesogenic monomer, Polymer Science U.S.S.R., 1984, 26, nº 12, 2882-2890.

[7]. A.Y. Bilibin,; S. S. Skorokhodov, Rational path of the synthesis of liquid-crystalline high molecular weight polyesters and their properties in solution, Makromol. Chem. Makromol. Symp. 1989, 29, 9-23.

[8]. M. Perez-Mendez; R. Marsal; L. Garrido; M. Martin-Pastor, Self-Association and Stereoselectivity in a Chiral Liquid-Crystal Cholesteric Polymer Formed under Achiral Conditions, Macromolecules 2003, 36, 8049-8055.

[9]. S. Sánchez-Cortés; R. Marsal-Berenguel; M. Pérez-Méndez, Adsorption of a Cholesteric Liquid-crystal Polyester on Silver and Gold Nanoparticles and Films Studied by Surface-Enhanced Raman Scattering, Applied Spectroscopy 2004, Volume: 58 Number: 5, pp: 562- 569.

[10]. M. Perez-Mendez; J. Fayos; G.P. Blanch; S. Sánchez Cortés, Biofunctionalization of Cholesteric Liquid-Crystal Helical Polymers. Nanocarriers, Encyclopedia of Nanoscience and Nanotechnology; Editor H. S. Nalwa; ACS. American Scientific Publishers; 2011, Volume 11, 547-580. (http://www.aspbs.com/enn/), ISBN: 1-58883-160-4.

[11]. M. Pérez Méndez; B. Hammouda, SAXS and SANS investigation of synthetic cholesteric liquid-crystal polymers for biomedical applications, Journal of Materials Science and Engineering B 3 (2) 2013 104-115.

[12]. M. Pérez Méndez; D. Rodriguez Martinez; S.M. King, pH-induced size changes in solutions of cholesteric liquid-crystal polymers studied by SANS, Journal of Physics: Conference Series 2014, 554, 012011, 1-11. Dynamics of Molecules and Materials-II, doi:10.1088/1742-6596/554/1/012011.

[13]. M. Pérez Méndez; D. Rodríguez Martínez; J. Fayos, Structure of non-viral vectors based on cholesteric liquid-crystal polymers by SAXS, International Journal of advancement in Engineering Technology, Management and Applied Science (IJAETMAS) November 2016, Volume 03 - Issue 11, pp. 27-41. ISSN: 2349-3224

[14]. http://www2.dupont.com/Products/en_RU/Kevlar_en.html.

[15]. National Cancer Institute Databases (NCI) Version 2001.1, https://gateway.discoverygate.com/CompLoc/secure/drilldown/top_fs.jsp

[16]. F. Freire; J. M. Seco; E. Quiñoá; R. Riguera, The Prediction of the Absolute Stereochemistry of Primary and Secondary 1,2-Diols by ^{1}H NMR Spectroscopy: Principles and Applications. Chem. Eur.J. 2005, Vol. 11, Issue 19, 5509-5522.

[17]. S. Arias; F. Freire; E. Quiñoá; R. Riguera, Nanospheres, Nanotubes, Toroids, and Gels with Controlled Macroscopic Chirality. Angew. Chem. Int. Edition 2014, 53, Issue 50:13720–13724.

[18]. Materials Studio Modeling v.2018, BIOVIA Cambridge, U.K. Inc.

[19]. D. Sek; A. Wolinska; H. Janeczek, Structure-liquid crystalline properties relationship of polyesteramides, J Polym Mater. 1986, 3, 225–233.

[20]. K. Goto; Y. Inoe, Poly(amide-ster) and method for its production, Patent 1996, Japan Synthetic Rubber Co Ltd, Japan CODEN: JKXXAF

[21]. J.C. Cobas; F.J. Sardina, Concepts Magn. Reson. 2003 19, 80-96.

[22]. MestReNova 11.0.4, Mestrelab Research SL, Santiago de Compostela, Spain, www.mestrelab.com, 2017.

[23]. C.A.G. Haasnoot; F.A.A.M. de Leeuw; C. Altona, The relationship between proton-proton NMR coupling constants and substituent electronegativities- I: An empirical generalization of the Karplus equation, Tetrahedron 1980, Vol. 36, Issue 19, 2783-2792.
[24]. H. Uzawa; Y. Nishida; H. Ohrul; H. Meguro, Application of the dibenzoate chirality method to determine the absolute configuration of glycerols and related acyclic alcohols, J. Org. Chem. 1990. 55. 116-122.
[25]. K. Ute; K. Hirose; H. Kashimoto; K. Hatada; O. Vogl, Haloaldehyde polymers. 51. Helix-sense reversal of isotactic chloral oligomers in solution, J. Am. Chem. Soc. 1991, 113, 6305- 6306, DOI: 10.1021/ja00016a076.
[26]. K. Ute; K. Oka; Y. Okamoto; K. Hatada; F. Xi; O. Vogl, Haloaldehyde Polymers LIII. Optical Resolution of Purely Isotactic Oligomers of Chloral: Optical Activity of the Chloral Oligomers Assuming One-Handed Helical Conformation in Solution, Polym. J., 1991, 23, 1419-1424.
[27]. K. Ute; K. Hirose; H. Kashimoto; H. Nakayama; K. Hatada; O. Vogl, Helix-Inversion Equilibrium of Isotactic Chloral Oligomers in Solution, Polym. J. 1993, 25, 11, 1175- 1186.
[28]. G. Tian; Y. Lu; B.M. Novak, Helix-Sense Selective Polymerization of Carbodiimides: Building Permanently Optically Active Polymers from Achiral Monomers, J. Am. Chem. Soc. 2004, 126, 4082-4083.
[29]. D.S. Schlitzer; B. M. Novak, Trapped Kinetic States, Chiral Amplification and Molecular Chaperoning in Synthetic Polymers: Chiral Induction in Polyguanidines through Ion Pair Interactions, J. Am. Chem. Soc. 1998, 120, 9, 2196-2197.
[30]. H.-Z. Tang; Y. Lu; G. Tian; M.D. Capracotta; B.M. Novak, Stable Helical Polyguanidines: Poly{N-(1-anthryl)-N‘-[(R)-and/or (S)-3,7-dimethyloctyl]guanidines}, J. Am. Chem. Soc. 2004, 126, 3722-3723.
[31]. M. Muller; R. Zentel, Interplay of Chiral Side Chains and Helical Main Chains in Polyisocyanates, Macromolecules 1996, 29, 1609-1617.
[32]. S. Song; S.A. Asher; S. Krimm; K.D. Shaw, Ultraviolet resonance Raman studies of trans and cis peptides: photochemical consequences of the twisted.pi.* excited state, J. Am. Chem. Soc. 1991, 113, 1155-1163.
[33]. M. Pérez Méndez, Synthetic Cationic Cholesteric Liquid Crystal Polymers, Liquid Crystals - Recent Advancements in Fundamental and Device Technologies, Chapter 2. (2018) 7-33, Ed. Pankaj Kumar Choudhury, InTech, DOI:10.5772/intechopen.70995. https://cdn.intechopen.com/pdfs-wm/58375.pdf.

Mercedes Pérez Méndez" Biocompatible, Nanostructured, Chiral Polyesteramides: PNOBDME $(C_{34}H_{38}N_2O_6)_n$ and PNOBEE $(C_{26}H_{22}N_2O_6)_n$ Synthesized and Characterised as Cholesteric Liquid Crystals." International Journal of Engineering Research and Applications (IJERA), Vol. 09, No.06, 2019, pp. 52-66